Dynamics of Forward Filtration Combustion at the Pore-Network Level

Chuan Lu and Yannis C. Yortsos
Dept. of Chemical Engineering, University of Southern California, Los Angeles, CA 90089-1211

DOI 10.1002/aic.10369

A pore-network model is developed, based on a dual lattice, to study the dynamics of forward filtration combustion (FC) in porous media at the pore-network scale. A novel moving coordinate method is also implemented that allows for the long-term profiles to be obtained in a straightforward manner. The model is used to reproduce recent analytical work, including the multiplicity of steady states for the nonadiabatic case, and to study a number of other effects. Particular emphasis is placed on the effect of the heterogeneity in the microstructure, introduced by the randomness in the pore radius. It is found that the local disorder leads to less oxidant consumption, as compared to the homogeneous case. This underprediction increases with an increase in the disorder, a decrease in the thermal conductivity, and a decrease in the spatial correlation. Temporary local extinction can result for sufficiently large injection rates. As a result of the heterogeneity, the spatially averaged reaction rate is generally different from the rate calculated based on the microscale Arrhenius expression, using the averaged variables, with discrepancies of a factor of 2 or higher not uncommon. Although this effect depends on the parameter values, it can be a cause of concern when the fronts at the small scale are sufficiently distorted. Coupling of fronts occurs in a layered system, when there is sufficient oxidant supply. These results show that the microscale geometry can have a strong influence on the overall macroscopic behavior of the process. © 2005 American Institute of Chemical Engineers *AIChE J,* 51: 1279–1296, 2005

Introduction

Filtration combustion (FC) is a process of importance to a variety of applications, ranging from the recovery of oil from oil reservoirs[1] to the processing of materials (see, for example, Hwang et al.[2,3]). In its most simplified form, it involves the combustion of a solid fuel deposited at the pore walls of a porous medium, through the injection of an oxidizing agent. When ignition occurs at the gas inlet, reaction and thermal fronts propagate in the direction of the injected gas, and the process is referred to as *forward FC*. When ignition occurs at the opposite side, the combustion front propagates in the direction opposite to the gas flow, and a process of reverse FC develops. In this paper, emphasis will be placed on forward FC.

A number of studies have addressed various features of FC. In the context of in situ combustion (ISC) for the recovery of oil, investigations have focused on issues, such as the detailed kinetics of the various reactions or the development of generally elaborate numerical simulators for field applications.[1] In situ combustion is a complex process, however, in that the solid fuel is generated in situ, and the transport and reaction environment is generally multiphase and multicomponent. As a result, many fundamental aspects of the process are still poorly understood. A better understanding has been achieved in the simpler problem of FC, in which the solid fuel is known a priori, and only a single gas phase is involved in fluid flow. Emphasis in this field has been paid almost exclusively to continuum models, however. Aldushin,[4] Shult et al.,[5] Aldushin and Matkowsky,[6] and Aldushin et al.[7] studied the properties of

---

Correspondence concerning this article should be addressed to Y. C. Yortsos at yortsos@usc.edu.

the propagation front (including front instabilities) based on an asymptotic analysis of the continuum model. Using an analogous framework, Akkutlu and Yortsos[8] investigated the effect of volumetric heat losses on steady-state multiplicity. The same group also addressed propagation in a layered system.[9] Reverse FC has been explored experimentally[10] and by some simple numerical models.[10,11]

In the conventional continuum models, variables such as reaction rates, concentrations, or temperatures are volume-averaged continuum variables. The validity of such approaches is based on the premise that spatial gradients are small at the scale of the microstructure, so that volume-averaged quantities are meaningful, and effective parameters reflect fairly accurately the actual process. Large gradients at the microscale, however, are possible for a number of reasons, including the development of sharp propagating fronts or of microscale instabilities. In forward displacement, such as of one fluid by another in a porous medium, fronts arise naturally, either because of viscous flow or because of instabilities at the small scale.[12] Sharp fronts are quite common in reaction–diffusion problems (see, for example, Edwards et al.[13] Edwards[14]). In forward FC (and ISC), sharp fronts are expected because of the small thickness of the reaction zone, resulting from the fast kinetics of the combustion reaction. Dissipation processes, such as diffusion and conduction, balance the reaction rates and lead to sharp fronts.[8] In reverse FC[10] the development of spatial instabilities is another cause of large gradients.

One concern that may arise in these cases is whether volume averages, such as those of the reaction rate (assuming that they can be defined) can be expressed by the same expressions as with the local ones (which represent the true kinetic expressions). For example, assuming that the latter have the conventional, nonlinear, Arrhenius dependency

$$r \propto C \exp\left(-\frac{E}{RT}\right) \tag{1}$$

the question exists whether the same volume-averaged relations apply, that is, whether the expression

$$\langle r\rangle = \langle C\rangle \exp\left(-\frac{E}{R\langle T\rangle}\right) \tag{2}$$

is also valid, when concentrations or temperatures vary significantly at the microscale.

One approach to addressing questions of this type is through small-fluctuation analyses, in which the relevant variables are expanded asymptotically in terms of the quantity that drives the nonuniformity, such as the variance in the flow permeability.[15] The equations obtained are subsequently linearized, and to leading order, expressions alternative to Eq. 2 are derived. Although very useful, such approaches have the limitation of the small fluctuation, and at present apply only to continuum models. For the problem of interest herein, a useful method for the understanding of the effect of the microstructure is direct pore-network modeling. This alternative is explored in this communication. We will develop a detailed pore-network model of the FC process, which we will then use to understand phenomena at the pore-network scale and derive conclusions about the process of forward FC.

The simulation of processes at the pore-network scale has emerged as a useful simulation tool for the understanding of fluid displacements in porous media. The approach relies on representing the porous medium by an equivalent network of sites and bonds, whose geometrical and transport characteristics derive from the pore microstructure. Sites (pores) are associated with volume, storage, or capacity, whereas bonds (pore throats) are associated with transport. Past models have been used to study isothermal, nonreactive flow and transport.[16] More recent works have extended the approach to nonisothermal systems, by considering a dual-lattice model.[17,18] Reactive transport has been simulated by pore networks in earlier works[19] in the context of acidization, and by Sahimi and Tsotsis[20] (see also Mann[21] and El-Nafaty and Mann[22]), in the context of catalyst coking and deactivation. Pore-network models of the FC process have been limited, however. Hwang et al.[2,3] developed a pore-network model of FC, but for a gasless system, in which the emphasis was on solid conduction. Transport in the pore space and the associate fluid flow and mass transfer were omitted. Nonetheless, the authors pointed out important effects of the local microstructure on the overall process. A similar model was used by the present authors to explore percolation phenomena in FC, when the fuel is distributed randomly.[23]

Discrete models for the full FC process, which account in detail for the pore microstructure, have not appeared in the literature, to our knowledge. This paper delineates our attempts to fill this gap. We will develop a pore-network model based on a dual lattice, which incorporates the relevant flow and transport processes. The description of the model and the related numerical scheme are detailed in the second section. In particular, we present a novel moving coordinate method in a random environment, to capture the moving combustion fronts at longer times. The model is then used to investigate the effect of the microstructure and its heterogeneity on forward FC and to probe the validity of the continuum approaches. Given that it can be viewed, under certain approximations, as an equivalent finite-difference analog of the continuum formalism, the pore-network model can also be used to probe larger-scale effects, as well. Concluding remarks are presented in the last section.

Mathematical Model

The pore-network model consists of a dual network of sites (pores) and bonds (throats), embedded in a network of solid sites, which are taken to represent the solid matrix (Figure 1A). The solid sites are needed to account for heat transfer in the inert solid matrix.[17] The pores are places where solid fuel exists and reaction occurs. They are interconnected by throats, which control transport of mass, momentum, and heat. Coupling of the solid and the pore space occurs through the heat transfer between pores and solid sites, as shown in Figure 1B. In the two-dimensional (2-D) simulations to be reported below, both networks are taken as square lattices. Three-dimensional (3-D) extensions are reported in Lu.[24]

Important features of the model include the following:

(1) Each solid site communicates with four other solid sites (depicted in Figure 1B by solid lines), by heat conduction, and with one pore site (the dashed line between solid and pore sites

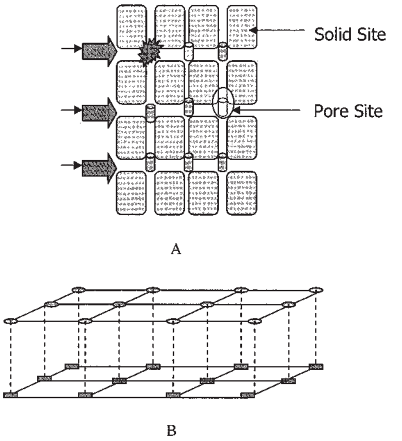

Figure 1. Thermally coupled pore network and the inert solid matrix.

(A) The pore network; (B) the coupling between the pore network and the solid lattice. Gray: pore network; black: inert solid; green: solid fuel. Dashed lines indicate pore–solid interactions.

in Figure 1B), by heat transfer from the pore space. A heat-transfer coefficient models the pore space–solid matrix thermal exchange.

(2) Injection of a mixture of oxidant (such as oxygen) and inert gas occurs at one end of the domain, where pressure, temperature, and composition are specified. The outlet end is at a constant pressure. Flow in the pore throats is governed by Poiseuille's law. The oxidant in the gas phase is delivered by gas-phase diffusion and convection.

(3) The following one-step heterogeneous reaction is assumed:

$$\text{Solid Fuel} + \mu \text{ Gas Oxidant} \rightarrow \mu_1 \text{ Solid product} + \mu_2 \text{ Gas Product} \quad (3)$$

where μ, μ_1, and μ_2 are stoichiometric coefficients for the corresponding pseudospecies. Implicit above is the assumption that the reaction is heterogeneous and does not involve the propagation of flame in the pore network. The kinetics have been vastly simplified to allow for a manageable numerical solution. However, more complex kinetics, including multistep, parallel, or serial schemes, could also be implemented. The reaction rate is expressed by the one-step kinetic model

$$R = k_r A_r P X_o H(V_f) \exp\left(-\frac{E_a}{RT}\right) \quad (4)$$

where H is the step function, V_f is the volume of fuel, P is the gas pressure, k_r is a kinetic constant, A_r is the gas–fuel interface area of an individual pore site, X_o is the mass fraction of the oxidant, and E_a is the activation energy.

(4) Within a pore site, thermodynamic equilibrium is assumed, and thus concentrations, pressure, and temperature are uniform. However, heat transfer does take place between adjacent pore sites, between pore and solid sites, and between adjacent solid sites. Thermodynamic and transport parameters will be taken constant for simplicity.

Governing equations

The governing equations express mass, momentum, and energy balances at the sites of the two lattices. They are as follows:

(1) Balances on pore site i, adjacent to pore sites denoted by j:

Gas-Phase Component k Mass Balance

$$\frac{\Delta\left(\frac{P_i V_i}{RT_i} y_{i,k} M_k\right)}{\Delta t} = -\sum_j u_{ij} r_{ij}^2 \frac{P_i y_{i,k}}{RT_i} M_k - \frac{D_e}{lR} \sum_j r_{ij}^2 \left(\frac{P_i + P_j}{2}\right) \times \left(\frac{2}{T_i + T_j}\right)(y_{i,k} - y_{j,k}) + \mu_k \left[k_r A_i^r \frac{P_i y_{i,O_2}}{RT_i} \exp\left(-\frac{E_a}{RT_i}\right)\right] H(V_{i,f}) \quad (5)$$

Fuel Balance

$$\rho_f \frac{\Delta V_{i,f}}{\Delta t} = k_r A_i^r \frac{P_i y_{i,O_2}}{RT_i} \exp\left(-\frac{E_a}{RT_i}\right) H(V_{i,f}) \quad (6)$$

Energy Balance

$$\frac{\Delta E_i}{\Delta t} = -\sum_j u_{ij} r_{ij}^2 \frac{E_{g,i}}{V_i} - \frac{\lambda_{gs}}{l} \sum_j r_{ij}^2 (T_i - T_j) - h_s \sum_s A_{is}^h (T_i - T_s) - h_{L,P} A_{i,l}^h (T_i - T_0) \quad (7)$$

where we defined the energy content of a site as

$$E_i = E_{f,i} + E_{g,i} \qquad E_{f,i} = \rho_f v_{f,i} (C_{p,f} T_i + \Delta_c H_f)$$
$$E_{g,i} = \sum_k \frac{P_i V_i}{RT_i} M_k y_{i,k} (C_{pg,k} T_i + \Delta_c H_f) \quad (8)$$

Momentum Balance

$$u_{ij} = \frac{r_{ij}^4}{8\kappa l} (P_i - P_j) \quad (9)$$

(2) Energy balance on solid site s, adjacent to solid sites denoted by s' and pore sites denoted by j:

Solid Site Energy Balance

$$\rho V C_{ps} \frac{\Delta T}{\Delta t} = -\frac{\lambda_s}{l} \sum_{s'} A_{ss'}^h (T_s - T_{s'}) + h_s \sum_j A_{js}^h (T_j - T_s) - h_{L,s} A_{s,l}^h (T_s - T_0) \quad (10)$$

We note the following: The sums in the energy balances express heat transfer between pore and solid sites, although we have also allowed for a volumetric heat loss to the surroundings, expressed through the heat transfer coefficient $h_{L,s}$. In addition, ideal gas behavior was assumed. Finally, the bond

Table 1. Notation Used

Variable	Notation	Typical Values
Temperature	T	Ambient 373 K
Pressure	P	Outlet 1.01×10^6 Pa
Bond length	l	5×10^{-4} m
Bond radius	r	$l/2$
Pore volume ratio	φ	0.3
Site reaction surface	A_i^r	l^2
Site heat transfer surface with surroundings	$A_{i,l}^h$	l^2
Site heat transfer surface with solid	$A_{i,s}^h$	l^2
Pore site volume	V	φl^3
Solid volume	V_s	$(1 - \varphi)l^3$
Fuel volume	V_f	$0.0077 l^3$
Pure fuel density	ρ_f	2.63×10^3 kg/m^3
Solid density	ρ_s	2.63×10^3 kg/m^3
Reaction rate	$k_0 = k_r \exp(-E_a/RT^*)$	4.1×10^8 kg m^{-1} mol^{-1} s^{-1}
Activation energy	E_a	73501.6 kJ/kmol
Heat of reaction	$\Delta_r H$	39452 kJ/kg
Stoichiometric coefficient	μ	3.018
Stoichiometric coefficient	μ_2	4.018
Solid heat capacity	$C_{p,s}$	1094 J kg^{-1} K^{-1}
Pure fuel heat capacity	$C_{p,f}$	1094 J kg^{-1} K^{-1}
Gas heat capacity	$C_{pg,k}$	1000 J kg^{-1} K^{-1}
Heat conductivity between pore sites	λ_{gs}	0.07 W m^{-1} K^{-1}
Heat conductivity between solid sites	λ_s	0.8655 W m^{-1} K^{-1}
Pore/surrounding heat transfer coefficient	$h_{L,p}$	0.8 W/m^2 K
Pore/solid heat transfer coefficient	h_s	8 W m^{-2} K^{-1}
Solid/surrounding heat transfer coefficient	$h_{L,s}$	0.8 W m^{-2} K^{-1}
Gas phase velocity	U	0.005 m/s
Diffusion coefficient	D_e	5×10^{-5} m^2/s
Gas viscosity	κ	17.3×10^{-3} cP

radius can be correlated to the depth of conversion (such as probing instability effects), although in the applications below, the radii were kept time invariant. Table 1 contains the detailed nomenclature associated with the above equations.

The equations were made dimensionless using the characteristic quantities and values listed in Table 1. The latter were obtained from Akkutlu[25] and correspond to typical parameters for in situ combustion. We note specifically that the bond characteristic length was taken as 500 μm, whereas injection rates were of the order of 100 m/day. Dimensionalization of the equations results in a number of dimensionless groups, including pore-scale Peclet and Nusselt numbers. The latter express heat transfer between the pore space and the solid, and the heat losses to the surroundings (see also below). Together with other parameters, such as the initial temperature, the volume ratio of solid site to the pore site, the average initial fuel amount in pore sites and the oxidant concentration at injection, the dimensionless parameters constitute the main set of variables affecting the process.

Remarks

- The above model allows for simulating both forward and reverse combustion. As noted above, these are differentiated through the control of the ignition location, which is the inlet row in the case of forward combustion, and the row before the outlet, in the reverse case (Figure 2). The emphasis in this work is on forward FC. Reverse combustion is discussed in a separate publication.[26]
- For the momentum balance we have assumed Poiseuille flow. At the continuum level, this is equivalent to Darcy's law, an assumption that is very often made in the literature. Furthermore, because of the linearity in the flow-rate/pressure-drop relationship in both models, the pore-network model can be also viewed, subject to appropriate modifications, as the finite-difference version of the continuum model, where Darcy's law applies.
- Radiation was neglected.
- The true kinetics of FC, and certainly of ISC, are quite complicated. For example, in the latter process, they can be accompanied by pyrolysis, evaporation and condensation, multistep reactions, and also by some gas-phase reactions.[27-29] At the same time, the simple one-step kinetics, as assumed above, are commonly accepted for the combustion of solid fuels.

The numerical scheme

The dimensionless formalism along with the appropriate boundary conditions was numerically solved using standard implicit schemes. In general, the equations were solved by a Newton–Raphson method. We used a variety of linear solvers, including a traditional SOR method, a preconditioned conju-

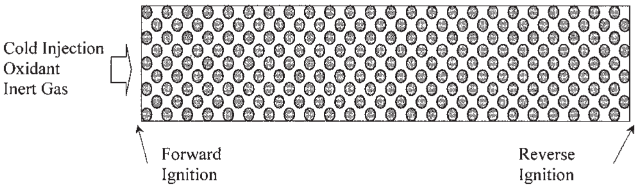

Figure 2. Schematic of filtration combustion.

Dark color denotes the solid fuel and the inert solid. The left end is the place of gas injection. For forward FC ignition occurs at the left end; for reverse FC ignition occurs at the right end.

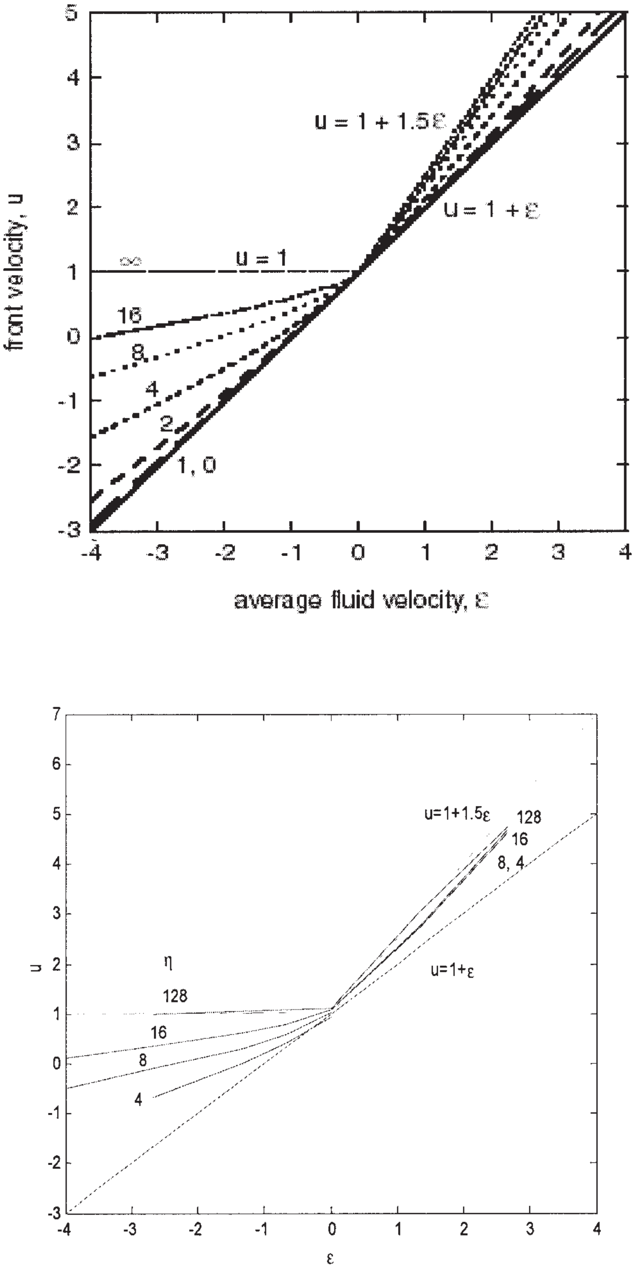

Figure 3. Dimensionless reaction front velocity *u* vs. the dimensionless average fluid velocity ε between parallel plates for the autocatalytic system of Eq. 13 and for different values of the Peclet number η.

The top panel is from Edwards[14]; the bottom panel corresponds to the numerical moving-coordinate method. The front velocity increases monotonically with increasing ε at fixed η.

gated gradient (PCCG) method, and LSOR methods, all of which can be effective for heterogeneous systems. These were used as appropriate.

Because of numerical dispersion, when the injection rate is relatively high [large Pe numbers: Pe $> O(10)$], special methods, such as an FCT scheme, in which artificial diffusion is used to smooth the shock, and a subsequent correction term to correct the flux, were adopted. An implicit predictor–corrector method was used for the temporal evolution. This method is 2nd-order accurate in time for most cases. Because of the stiffness of the problem and the associated small length scale, however, time steps were small (and typically confined to <1 s). To speed up computations, further simplifications were necessary. To this effect, we introduced the following assumptions:

(1) *Constant pressure*. Because the gas viscosity is small, pressure variations can be ignored in all of the governing equations, except in Poiseuille's law (Eq. 9). The assumption is justified by the fact that the velocities are much smaller than the speed of sound. It is widely used in the simulation of laminar flames in open space. The computational advantages are that the momentum equation becomes decoupled, and the continuity equation linearized with respect to pressure.

(2) *Quasi-steady state in the gas phase*. Because of the difference in the densities of gas and solid, the corresponding timescales are substantially different,[30] and thus the transient terms can be neglected in the gas mass balance equation.[6] Slow convergence may occur, such as when the solid fuel becomes depleted. Then, the time step is reduced and additional iterations are needed, for instance as in the PICO technique.[31,32] Instead of setting a constraint on the number of iteration times as done in the latter, however, we reduced the time step—if convergence cannot be reached after five iterations—to maintain accuracy. Numerical simulation results showed that use of all these assumptions dramatically decreases the computation time, without loss of accuracy in the pressure, temperature, and concentration profiles. Additional details can be found in Lu.[24]

A moving-coordinate method

In isothermal reaction systems, such as acidization or autocatalytic reactions, one is concerned with only one front, where concentrations change rapidly. In forward FC, both reaction and thermal fronts develop, in general with different widths.[8] In either case, the process reaches an asymptotic state consisting of a traveling wave, where the variables approach a constant profile, in the case of a homogeneous system, or become fluctuating functions around a mean profile, in the case when the microstructure is stochastic. Tracking the fronts until an asymptotic state is reached requires large computational domains and associated prohibitive computational costs. A way to circumvent this difficulty is to use a frame of reference that moves with the front. Such a technique was implemented in the paper. The novelty is that it was developed for a system whose parameters, such as the pore size, are random functions of space.

Consider the change of variables to a moving coordinate system, moving with velocity u. Parameters associated with the pore network are generally random variables in space, and in a moving coordinate ξ will necessarily become random variables in time, as

$$k(x, y) = k\left[\xi + \int_0^t u(t)dt,\ y\right] \tag{11}$$

If the parameters of the network are dependent on only the transverse location y, then a true traveling steady state devel-

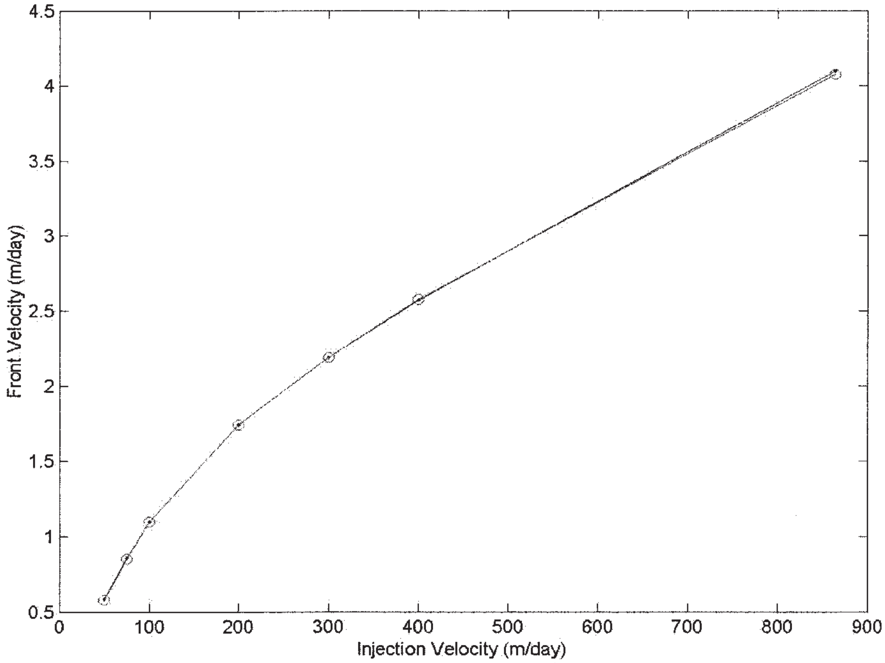

Figure 4. Asymptotic front velocity vs. the injection velocity in 1-D forward FC.

Blue denotes the analytical predictions by Schult and Matkowsky[5]; red denotes the results from our 1-D numerical simulation.

ops, in which the front velocity is constant and steady-state profiles are reached. An example will be shown below. However, if they also depend on the axial coordinate x, a true traveling steady state does not develop. In the traveling frame of reference, the system "sees" a fluctuating input, such as in the form of the fluctuating pore size. Then, at the asymptotic limit, variables, such as concentration, become fluctuating functions of time. In the moving coordinates, the only modification needed in the governing equations is the convective term associated with the change of the frame of reference. In addition, the boundary conditions in the moving coordinates must be modified. In particular, at the upstream boundary, we applied the boundary condition

$$y = y_0 \qquad \frac{\partial^2 T}{\partial x^2} = 0 \tag{12}$$

which is similar to the approach taken by Chen and Meiburg[33] in modeling miscible fingering in a tube. The front velocity is determined by requesting that the location of the front is maintained at a fixed point, arbitrarily selected, in the computational domain of the moving coordinate system. We defined the front by specifying that the *transverse average*, such as that of the conversion efficiency, takes a specific value at a fixed axial location. This will lead to a fluctuating asymptotic front velocity (see Lu[24] for more details).

The moving-coordinate method was validated with a comparison to the simpler autocatalytic system, in which only reaction fronts develop (see, for example, Edwards[14]). Here, the associated reaction–diffusion–advection equation is expressed as

$$\frac{\partial c}{\partial t} + \vec{v} \cdot \nabla c = \frac{1}{\eta} \nabla^2 c + 2\eta c^2(1 - c) \tag{13}$$

in which v is the flow rate, η is an equivalent Peclet number, and a cubic reaction rate was used. Note the autocatalytic nature of the rate expression. Variability in space is through the velocity term. For flow between two parallel plates, at $x = \pm 1$, this is the Poiseuille velocity profile

$$v(x, t) = \frac{3}{2} \varepsilon(1 - x^2) \tag{14}$$

where ε is the average fluid velocity in the direction of flow. The problem admits a traveling steady state, which is the solution of

$$\frac{1}{\eta}\left(\frac{\partial^2 c}{\partial \xi^2} + \frac{\partial^2 c}{\partial y^2}\right) + \left[u - \frac{3}{2}\varepsilon(1 - y^2)\right]\frac{\partial c}{\partial \xi} + 2c^2(1 - c) = 0 \tag{15}$$

Edwards[14] solved the above equation analytically in the limit of large Peclet numbers and numerically in the general case. A comparison between his results, for the dependency of the front velocity on the fluid velocity, and the results obtained by our moving-coordinate method, is shown in Figure 3 with η as parameter. The agreement is very good. Excellent agreement was also found for the concentration and the front profiles, as discussed in Lu.[24]

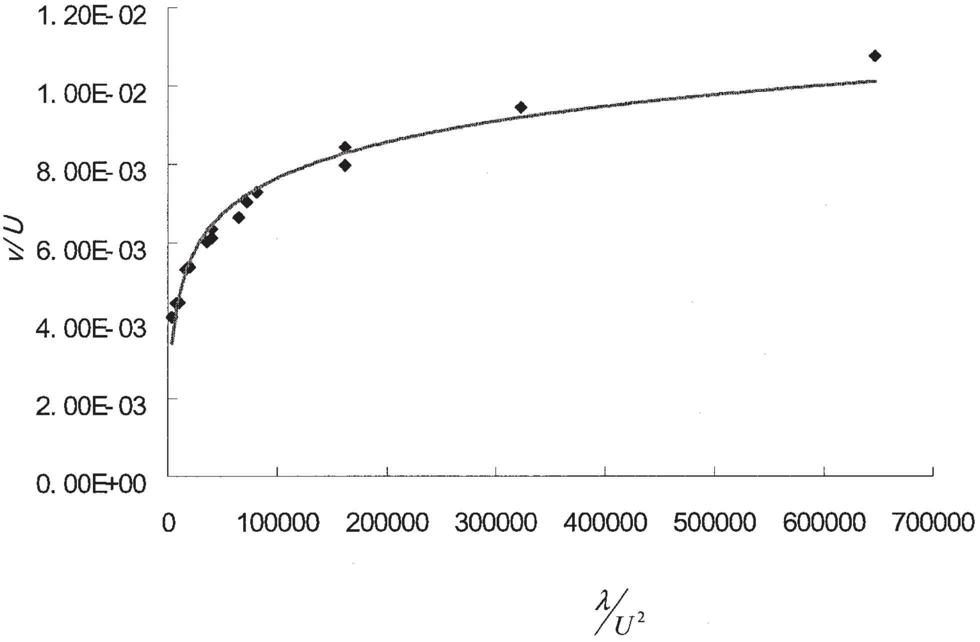

Figure 5. Effect of thermal conductivity on the front velocity in 1-D forward FC for different injection velocity and for the parameters of Table 1.

Red curve: analytical solution; blue diamonds: numerical results.

Although we do not have an exact result to assess the effectiveness of our method for randomly fluctuating systems, the above agreement gives us confidence that the moving coordinate method can be used successfully even in such cases. It was used in the results to be shown in the next section.

Results and Discussion

Forward FC in a homogeneous system

Before embarking on the general investigation of the 2-D forward FC in a heterogeneous pore network, we conducted a

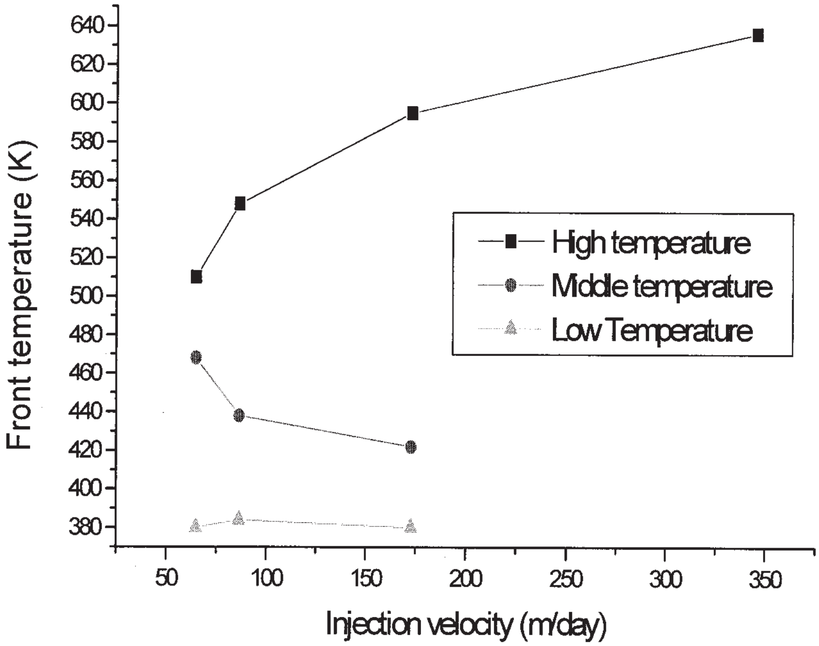

Figure 6. Multiple steady-state solutions for the front temperature (stable upper and lower branches and unstable intermediate branch) for the nonadiabatic case in 1-D forward FC as a function of the injection velocity and for the parameters of Table 1 (with heat loss Nusselt number equal to 2 × 10^{-4}).

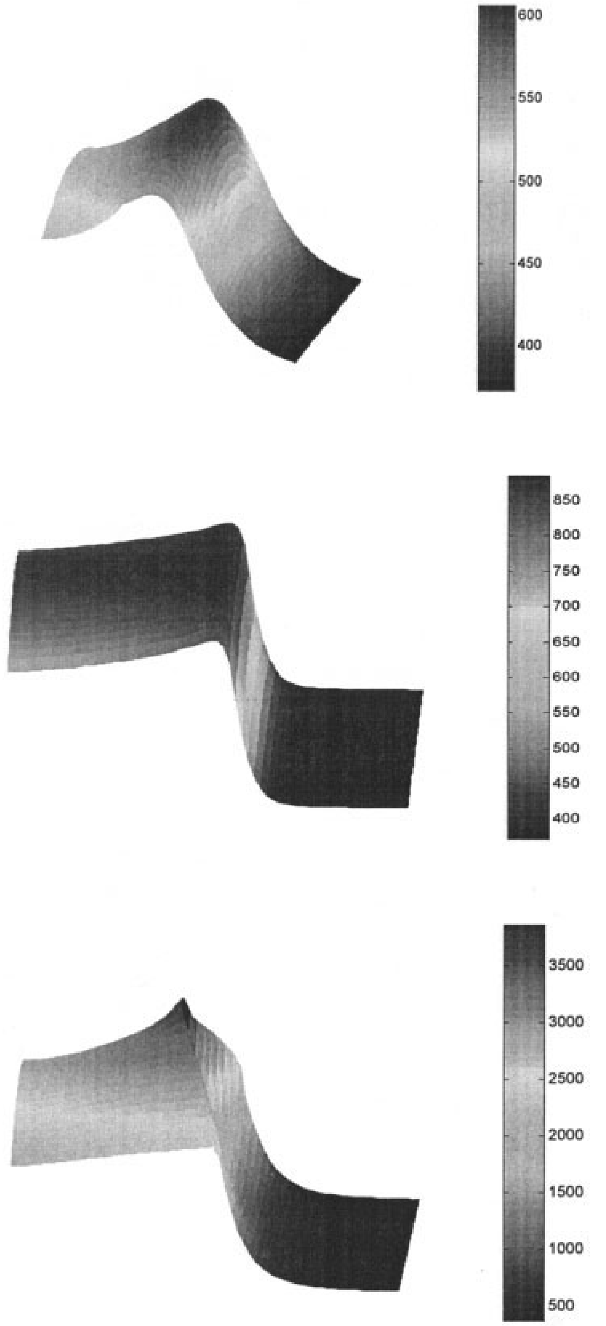

Figure 7. Temperature profiles (in degrees Kelvin) of forward FC in a 2-D domain with heat losses occurring at the lateral boundaries for Nu = 0.005.

Parameters from Table 1 with injection velocity 432 m/day, and fuel density equal to 5.83, 19.96, and 80 kg/m^3, from top to bottom, respectively.

study in a homogeneous system. Both adiabatic and nonadiabatic cases were examined. First, we focused on the simpler 1-D models, for which analytical results exist.[7,8] One should also keep in mind that the linearity in the flow-rate/pressure-drop relationship in the pore-network model allows us to also use it as a substitute (with some modification) of the numerical solution (finite-difference) of the continuum model. Deriving numerical solutions in this case would also help to support the validity of the model.

Aldushin et al.[7] showed the existence of three different structures, controlled by the value of the dimensionless parameter $\delta = c_g \mu \rho_{f0} / C_s a_0$: a reaction-leading pattern ($\delta < 1$), where the reaction front leads the thermal front; a reaction-trailing pattern ($\delta > 1$), where the reaction front trails the thermal front; and a pattern of maximum energy accumulation ($\delta = 1$), in which the two fronts coincide and the temperature at the front increases with time. Our numerical results (not shown here for the sake of brevity, but discussed in detail in Lu[24]) were found in excellent agreement with the theoretical predictions.

Of most interest to forward FC in our context is the reaction-leading case ($\delta < 1$). In such cases, Akkutlu and Yortsos[8] derived the following expression for the dimensionless front velocity V_D (made dimensionless with the injection velocity):

$$V_D^2 = \mathrm{A}\theta_f \exp\left(-\frac{\gamma}{\theta_f}\right)\left(\frac{1-\mu V_D}{1+\mu_g V_D}\right) \tag{16}$$

where the dimensionless front temperature θ_f is determined by the adiabatic front temperature

$$\theta_f \approx 1 + q \tag{17}$$

for an adiabatic system, and given by the expression

$$\theta_f \approx 1 + \frac{q}{\sqrt{1 + \frac{4h}{V_D^2}}} \tag{18}$$

for a system with convective heat losses. Here, we defined $\mathrm{A} = \tilde{a}_s \alpha_s k_0 Y_i \tilde{p}_i / qEv_i^2$, $\gamma = E/R\tilde{T}_0$, where h is a dimensionless heat-transfer coefficient. It is noted that Eqs. 17 and 18 are only approximate expressions, in that a weak dependency on velocity has been omitted. For future reference, we also note that forward FC is bound between two different regimes, a stoichiometric and a kinetic control regime. Stoichiometric control is obtained at large A (such as small injection velocities): as Eq. 16 shows, the dimensionless front velocity in this case approaches the constant

$$V_D = \frac{1}{\mu} \tag{19}$$

that is, in this limit the dimensional velocity is proportional to the injection velocity. The kinetic control is reached in the opposite limit of small A, in which case the front velocity approaches the limit

$$V_D^2 = \mathrm{A}\theta_f \exp\left(-\frac{\gamma}{\theta_f}\right) \tag{20}$$

and the dimensional front velocity becomes constant. These two limits will be further discussed below.

The 1-D Adiabatic Case. Consider, first, the adiabatic case.

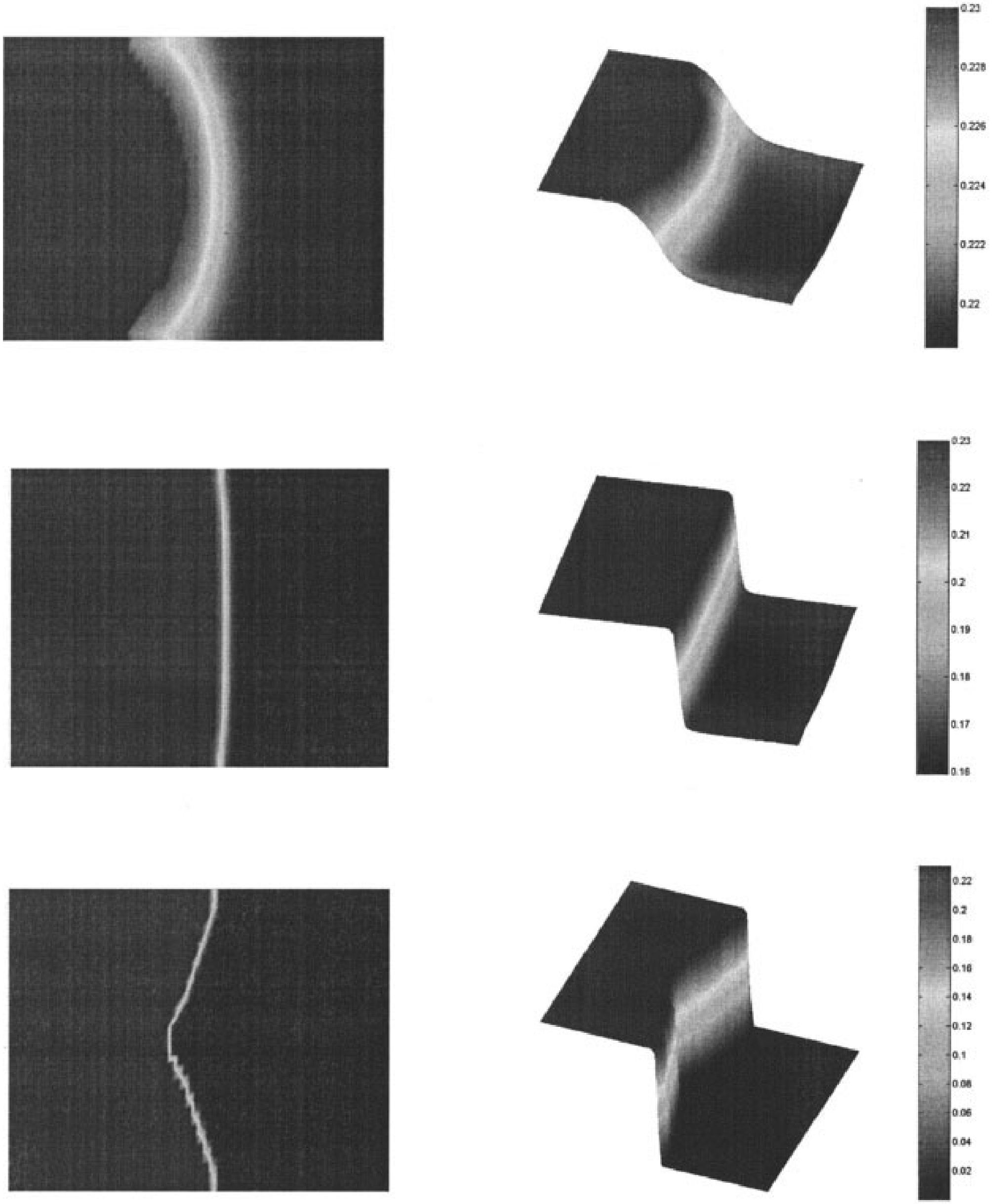

Figure 8. Conversion depth and mole fraction (concentration) profiles of forward FC in a 2-D domain with heat losses occurring at the lateral boundaries for Nu = 0.005.

Parameters from Table 1 with injection velocity 432 m/day, and fuel density equal to 5.83, 19.96, and 80 kg/m^3, from top to bottom. respectively.

Figure 4 shows a comparison of the results between theory and simulation for the dependency of the asymptotic (dimensional) front velocity on the injection velocity. The agreement is very good. The above two regimes of stoichiometric and kinetic control correspond to large and small values of the injection velocity, respectively (the kinetic control was not reached yet in the simulations in the figure). Similarly, good agreement was found for the other relevant variables, such as front temperature and oxidant consumption.[24]

Equation 16 shows that, in the 1-D case, a number of parameters affect the process only through the dimensionless group A. For example, the effect of conductivity on the dimensionless front velocity enters in the combination (conductivity) × (injection velocity)$^{-2}$. Equation 16 shows that an increase in the thermal conductivity is equivalent to a proportional decrease in the square of the injection velocity. We tested the theoretical predictions by using the numerical model. Figure 5 shows that a good agreement exists between theory and simulation. Because thermal conductivity affects the amount of oxidizer that could penetrate the reaction front, it has concomitant effects on front velocity. The effect of conductivity has significant ramifications to the full 2-D problem, as will be shown later.

The 1-D Nonadiabatic Case. Consider, next, the nonadiabatic case. Heat losses to the surroundings, in a direction perpendicular to the plane of front propagation (which thus

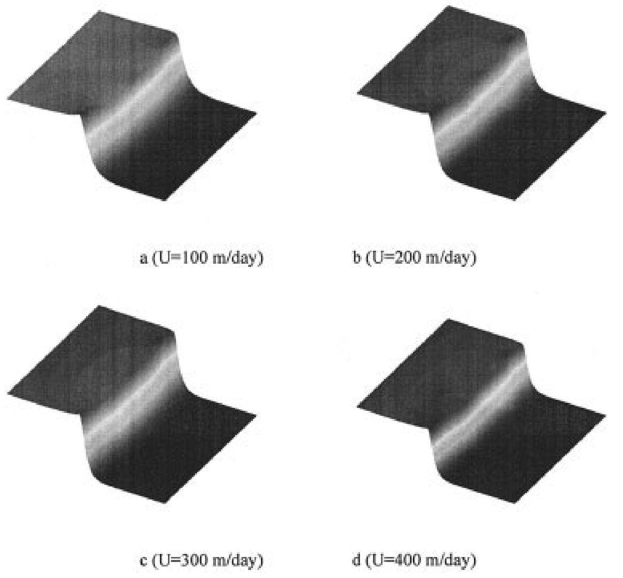

Figure 9. Temperature profiles in 2-D adiabatic forward FC for different injection velocity with white noise–distributed bond radius in the interval [0.2, 1.8], and for the parameters of Table 1 (thermal conductivity = 0.8635 W m^{-1} K^{-1}).

From top to bottom, the injection velocity varies between 100 and 400 m/day.

correspond to volumetric heat losses in the thermally thin limit for a 2-D geometry) were incorporated in the continuum model of Akkutlu and Yortsos,[8] who considered both convective and conductive modes. These authors showed that in the nonadiabatic case, the system exhibits a classical steady-state multiplicity, consisting of two stable branches (low and high temperature, respectively) and an intermediate unstable one. The corresponding S-shaped curve can be used, among other things, to provide ignition and extinction criteria. The validity of the theory for the convective heat loss mode (expressed here through an associated Nusselt number) was tested using the numerical model. The numerical results in Figure 6 show a multiplicity very similar to the analytical solution. In the numerical construction, the two stable branches were obtained by using different ignition temperatures. The intermediate, unstable branch was obtained by trial and error, as the dividing boundary between the two states, and may be subject to numerical error. The sensitivity of the multiple steady states to parameters, such as the heat loss rate and the injection velocity, was analyzed in detail in the work by Akkutlu and Yortsos,[8] to which the reader is referred for further details. Here, we will only point out that Lu[24] also found agreement between analytical and numerical results with respect to parameters such as the ignition temperature, which decreases with an increase in the injection rate and increases with the heat loss intensity, as expected.

The 2-D Nonadiabatic Case (Heat Losses from a Lateral Boundary). When heat losses are not volumetric, but occur only from a lateral side, they will affect the temperature distribution, possibly leading to a nonuniform profile. We considered the analysis of such cases, by simulating the process in a rectilinear geometry (Figures 7 and 8). Again, this analysis is also valid for the continuum model, given an appropriate correspondence in the magnitude of the dimensionless groups. A particularly important aspect as a result of such imposed boundary condition is the effect of gas-phase compressibility.

Nonuniform temperature profiles lead to two competing effects. Higher temperatures are associated with higher rates of reaction and, in 1-D, with higher front velocities. On the other hand, because of thermal expansion at higher temperatures, the mass supply of the oxidant decreases, thus leading to a competing retardation effect. This effect, which is pronounced only at high temperatures, can act to stabilize temperature perturbances. Thus hot spots may not necessarily travel faster. The effect may be important in SHS (self-propagating high-temperature synthesis) processes in which the front temperature is usually quite high (several thousand degrees Kelvin) and planar reaction fronts are necessary to maintain product quality.

To illustrate these effects, we conducted simulations using the data of Table 1, but in which we also varied the fuel density to achieve high temperatures. In all simulations heat loss occurred from the lateral boundary only. Figures 7 and 8 show temperature, conversion depth, and concentration profiles for three different values of the fuel density (5.83, 19.96 and 80 kg/m^3, respectively). When the fuel density is low, temperatures are generally low, the flow resistance caused by gas phase thermal expansion is weak, the gas phase reactant is not totally consumed even at the higher temperature center region, and a parabola-like profile forms, as a result of the balance of heat production and heat sink at the boundary. As the fuel density increases, however, the gas expansion effect becomes more significant. In the center, where temperatures are higher, the mass flux is retarded with respect to the sides, the oxidant supply is smaller, and thus front temperature, concentrations, and conversion depth profiles become more uniform. As the density increases even further, the even higher front temperatures cause the system to depart from kinetic control to stoichiometric control, in which case the gas supply becomes the dominant factor. The region of higher temperature is subject to a significant, compressibility-induced retardation of the oxidant supply, causing the center temperatures to lag compared to the sides. As a result, the front acquires a concave rather than a convex shape (Figures 7 and 8). We point out that these profiles become stationary in the moving coordinate system at longer times. The transition between the profiles is interesting and should be the subject of a future study.

Forward FC in a 2-D heterogeneous system

An important objective of any pore-network modeling study is the understanding of how microscale heterogeneity can affect macroscale properties. Heterogeneity can be introduced in a number of ways, such as through the distribution of permeability, the heat conductivity, or the fuel amount. The effect of a distributed fuel amount is quite interesting because it may involve percolation phenomena, and it is discussed in a separate publication.[23] Here, we will focus on the effect of the pore-size distribution, which primarily affects the flow field through the Poiseuille flow conductance of the pore throats, but also the concentration through diffusion in the pore space, the conductance of which also depends on the pore radius. We will take three different heterogeneity modes for the pore size distribution: white noise (spatially uncorrelated), fractional

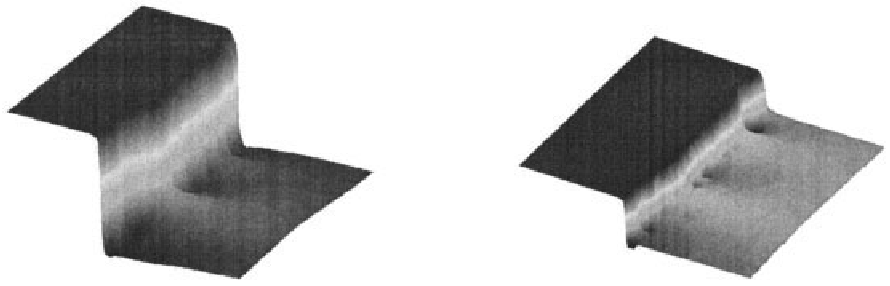

a (U=100 m/day) b (U=200 m/day)

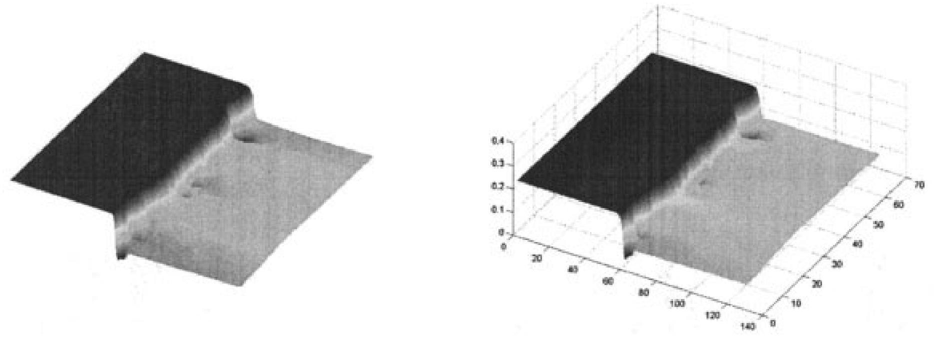

c (U=300 m/day) d (U=400 m/day)

Figure 10. Concentration profiles in adiabatic 2-D forward FC for different injection velocities with white noise–distributed bond radius in the interval [0.2, 1.8], and for the parameters of Table 1 (thermal conductivity = 0.8635 W m^{-1} K^{-1}).

From top to bottom, the injection velocity varies between 100 and 400 m/day.

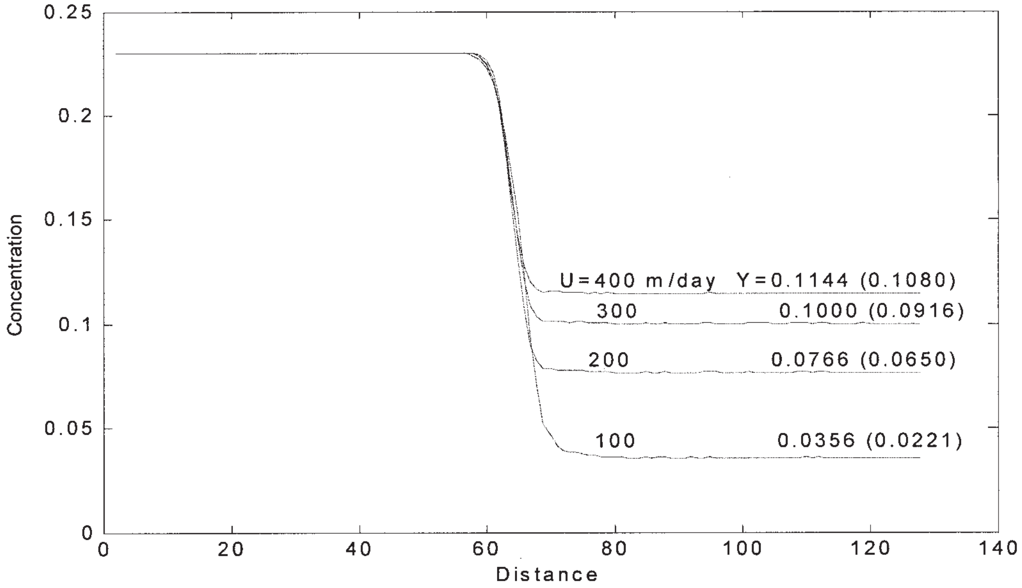

Figure 11. Transversely and time-averaged mole fraction profiles in adiabatic 2-D forward FC for different injection velocities with white noise–distributed bond radius in the interval [0.2, 1.8], and for the parameters of Table 1 (thermal conductivity = 0.8635 W m^{-1} K^{-1}).

The values in parentheses are from the 1-D homogeneous solution.

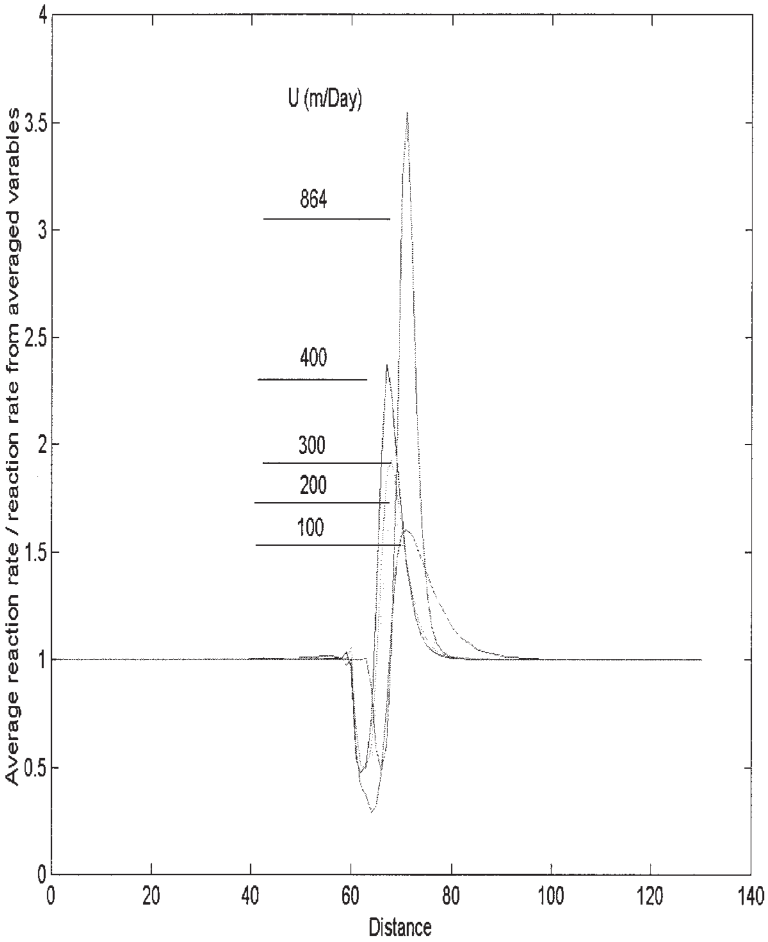

Figure 12. Spatial profiles of the ratio of the average reaction rate to the calculated reaction rate using the Arrhenius expression with the averaged concentration, fuel density, and temperature, as a function of the injection rate.

Adiabatic 2-D forward FC with white noise–distributed bond radius in the interval [0.2, 1.8] and for the parameters of Table 1 As the injection rate increases, the difference between the actual and the effective continuum rates increases, illustrating the combined effects of Peclet number and heterogeneity.

Brownian motion (fBm)[34] (spatially correlated), and a two-layered system. The effect on the macroscale quantities will be quantified using transverse averaging of the variables, such as concentration and temperature, followed by time-averaging to smooth out fluctuations.

White Noise–Distributed Pore Sizes. In this and the subsequent sections we will report adiabatic FC simulations in a 128×64 pore network. First, we considered pore sizes distributed as a white noise, from a uniform distribution in the interval [0.2, 1.8]. An asymptotic state in the moving coordinate system is ultimately reached, in which all quantities fluctuate near the front. Figures 9 and 10 show snapshots of the corresponding temperature and concentration profiles. The effect of disorder is different in the temperature and concentration profiles. The temperature profile, although sharp near the front, is quite smooth, reflecting the very effective heat conduction. For the given value of thermal conductivity, the stabilizing effect of conduction is dominant at the pore-network scale, thus smoothing out the temperature front. On the other hand, the concentration profile is more sensitive to the disorder and shows notable 2-D features. In particular, one notes nonuniform oxidant consumption, with places where there is more oxidant leakage through the front, and others where there is relatively higher consumption. Both these features intensify when the injection velocity is increased. Consistent with the 1-D analysis, the oxidant consumption is higher when the injection velocity is lower. The associated time- and transversely averaged mole fraction profiles are shown in Figure 11 for different values of the injection rate. We note that the 2-D averages underpredict the oxidant consumption, although not to a very substantial degree. The discrepancy arises from the nonuniformity in the velocity field, resulting from the pore throat radius disorder.

Although the averaged variables do not vary significantly from their homogeneous counterparts, the corresponding reaction rate profiles are quite different. Figure 12 shows that the reaction rate expressed in terms of the averaged variables can be several times different (faster, or slower), than the actual, depending on location. Near the reaction front, the macroscopically based reaction rate is two times larger than the actual, on the upstream side, and almost four times smaller than the actual, on the downstream side. The effect is influenced by the

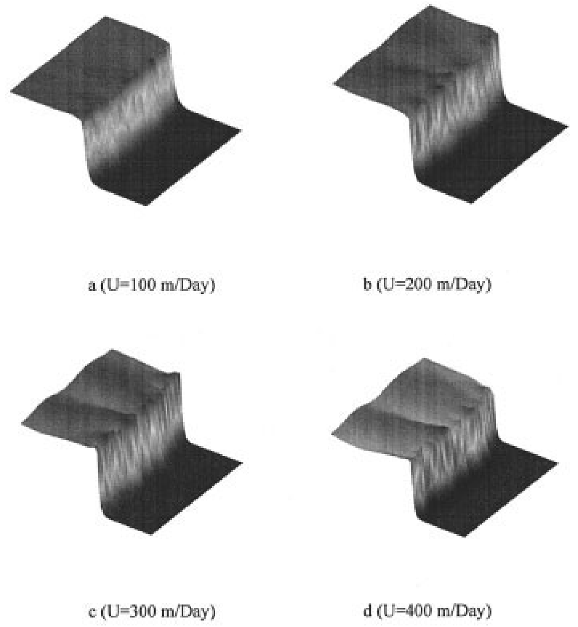

a (U=100 m/Day) b (U=200 m/Day)

c (U=300 m/Day) d (U=400 m/Day)

Figure 13. Temperature profiles in adiabatic 2-D forward FC for different injection velocities with white noise–distributed bond radius in the interval [0.01, 1.99], and for the parameters of Table 1 (thermal conductivity = 0.08635 W m^{-1} K^{-1}).

From top to bottom, the injection velocity varies between 100 and 400 m/day.

injection rate: the larger the injection rate, the larger the difference. This is attributed to the decrease of the relative strengths of diffusion at higher injection rates. Clearly, the use of the Arrhenius expression with averaged variables to estimate the average rate can result in serious errors. Even so, the resulting effect on the prediction of the overall performance (such as oxidant consumption, front temperatures, and front velocities) is relatively weak for this set of parameters. We point out that the width of the reaction front does not exceed a relatively finite number of pores (of the order of 20 for this set of parameters). This narrow width is consistent with the continuum analysis,[8] where widths not exceeding a few centimeters are predicted.

The effect becomes significantly more pronounced, however, when the thermal conductivity decreases and/or the bond size distribution is wider. Results for the same set of parameters, but with the thermal conductivity reduced by a factor of 10, and a wider pore-size distribution, in the interval [0.01, 1.99], are shown in Figures 13–16. Heterogeneity induces a significant effect not only on concentration but also on the temperature profiles. The front width decreases compared to the previous. We note the existence of temporary, fluctuating hot spots, temporarily unreacted sites, consistent oxidant leaks, and nonuniform reaction fronts, with the nonuniformity increasing with an increase in velocity. These features fluctuate with time in the moving-coordinate system, and inactive sites become active, given that the fuel is ultimately fully consumed. (This is in contrast to the case of reverse combustion; see Lu and Yortsos,[26] where unburned fuel is bypassed). Comparison with the 1-D continuum model shows that the front temperature is consistently underpredicted, whereas the consumption of the oxidant is consistently overpredicted (see Lu[24]). The figure equivalent to Figure 11, omitted here for the sake of brevity, shows that the oxidant mole fraction downstream of the front is overpredicted by at least a factor of 2. This is a result of poor thermal conduction and poor mass diffusion, which cause the emergence of sparse hot spot activities in various areas of the front, with a concomitant increase in temperature. Figure 15 shows that in this case, trying to estimate the effective reaction rate using macroscopic variables can lead to dramatic errors, which can reach as high as an order of 10^3 in certain places. Figure 16 is another illustration of this effect based on a 2-D profile of the reaction rate. In this case of low thermal conductivity, higher injection rates can cause localized, temporary extinction. Because reacting spots with more oxygen supply propagate faster than others with less oxygen supply, once a spot departs from the averaged front motion, the corresponding heat loss causes temporary extinction, inducing a concomitant oxygen leakage and a rougher front, as shown in the figures.

A different way of interpreting the results of this section is by considering the disorder-induced length scale, which is roughly the standard deviation of the pore-size distribution. If this scale is comparable to the characteristic scale for diffusion and conduction, then nontrivial phenomena, such as localized extinction and incomplete oxidant consumption, will take place.

fBm-Distributed Pore Sizes (Spatially Correlated Systems). A similar behavior exists in spatially correlated systems. To

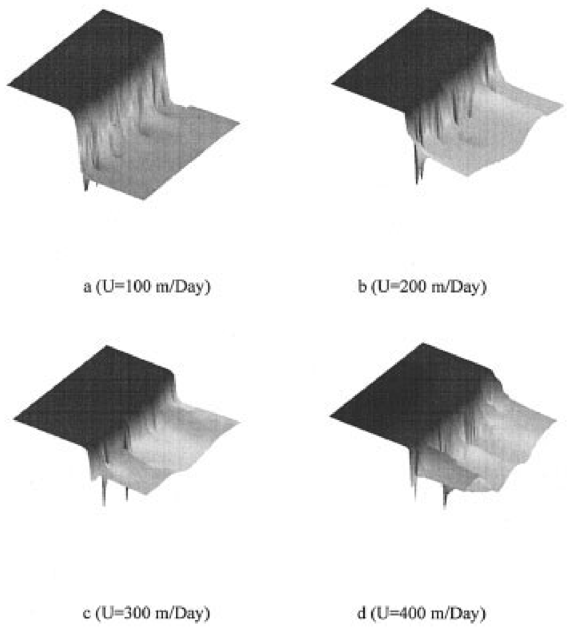

a (U=100 m/Day) b (U=200 m/Day)

c (U=300 m/Day) d (U=400 m/Day)

Figure 14. Concentration profiles in adiabatic 2-D forward FC for different injection velocities with wide white noise–distributed bond radius in the interval [0.01, 1.99], and for the parameters of Table 1 (thermal conductivity = 0.08635 W m^{-1} K^{-1}).

From top to bottom, the injection velocity varies between 100 and 400 m/day.

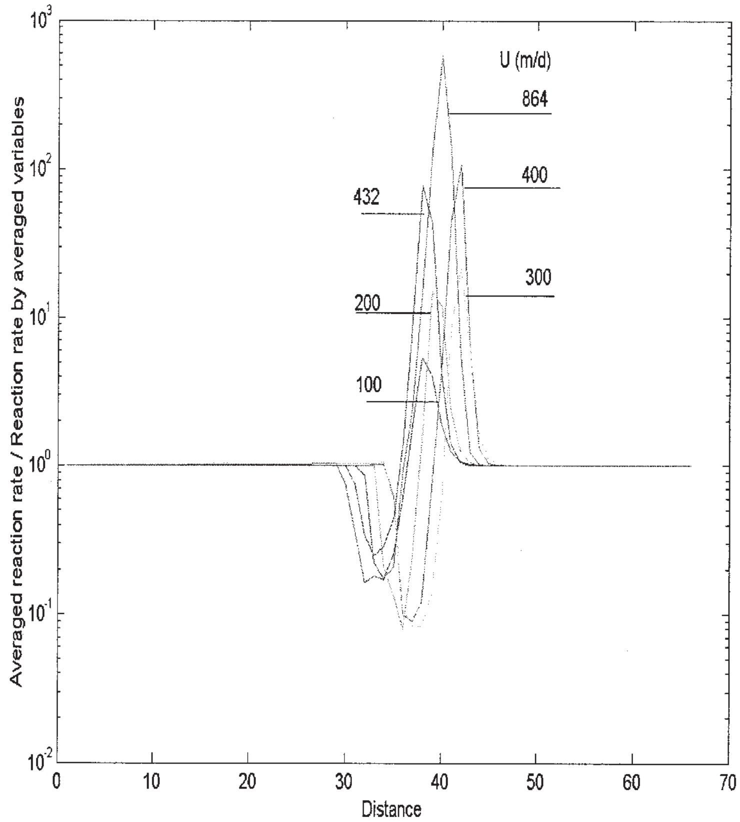

Figure 15. Spatial profiles of the ratio of the average reaction rate to the calculated reaction rate by averaged concentration, fuel density, and temperature as a function of the injection rate.

Adiabatic 2-D forward FC with wide white noise–distributed bond radius in the interval [0.01, 1.99], and for the parameters of Table 1 (thermal conductivity = 0.08635 W m^{-1} K^{-1}). As the injection rate increases, the difference between the actual and the effective continuum rates increases, illustrating the combined effects of Peclet number and heterogeneity. The effect is much larger than that shown in Figure 12, indicating the decreasing importance of mass diffusion and heat conduction.

investigate spatial correlation effects, we conducted simulations where the pore radius was distributed based on fractional Brownian motion (fBm) statistics, which display spatial correlations at all scales. Such distributions are characterized by a parameter, the Hurst exponent H, where $0 < H < 1$, with higher values of H reflecting a smoother and more correlated field. In the examples to be shown below, we considered two different injection velocities (100 and 432 m/day) and two different thermal conductivities, which differed by a factor of 10 (λ = 0.08655, and 0.8655 W m^{-1} K^{-1}, respectively). For the system with the higher thermal conductivity, the results were not very different from the random system discussed earlier. Concentration and temperature profiles were affected to some degree, with the more correlated system closer to the 1-D solution (see Lu[24] for more discussion). Even though some perturbations existed in the concentration profiles, however, both the asymptotic upstream temperature and the downstream concentration did nor differ notably from the homogeneous 1-D process. Nonetheless, the difference between the averaged rate and the rate calculated with the averaged parameters persisted in much the same way as in the previous random case (Figure 17). This difference was found to decrease with increasing values of H, that is, as the system becomes more correlated and the heterogeneity smoother. The smoothing effect of higher spatial correlation is expected.

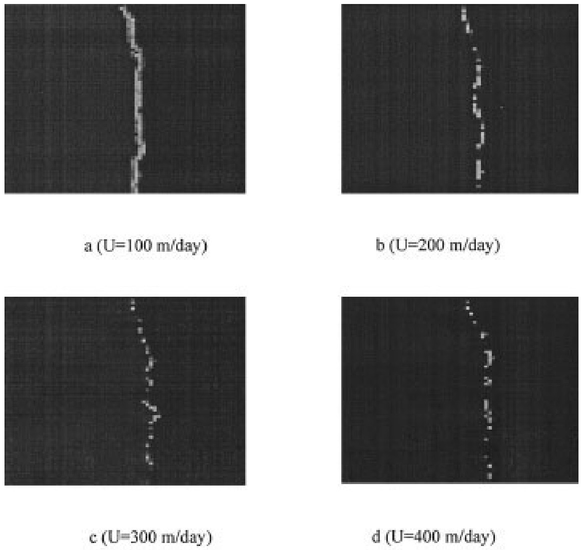
a (U=100 m/day)
b (U=200 m/day)
c (U=300 m/day)
d (U=400 m/day)

Figure 16. Spatial profiles of the reaction rate as a function of the injection rate.

Adiabatic 2-D forward FC with wide white noise–distributed bond radius in the interval [0.01, 1.99] and for the parameters of Table 1 (thermal conductivity = 0.08635 W m^{-1} K^{-1}). As the injection rate increases, the number of ignited sites at any given time decreases, leading to incomplete oxidant consumption.

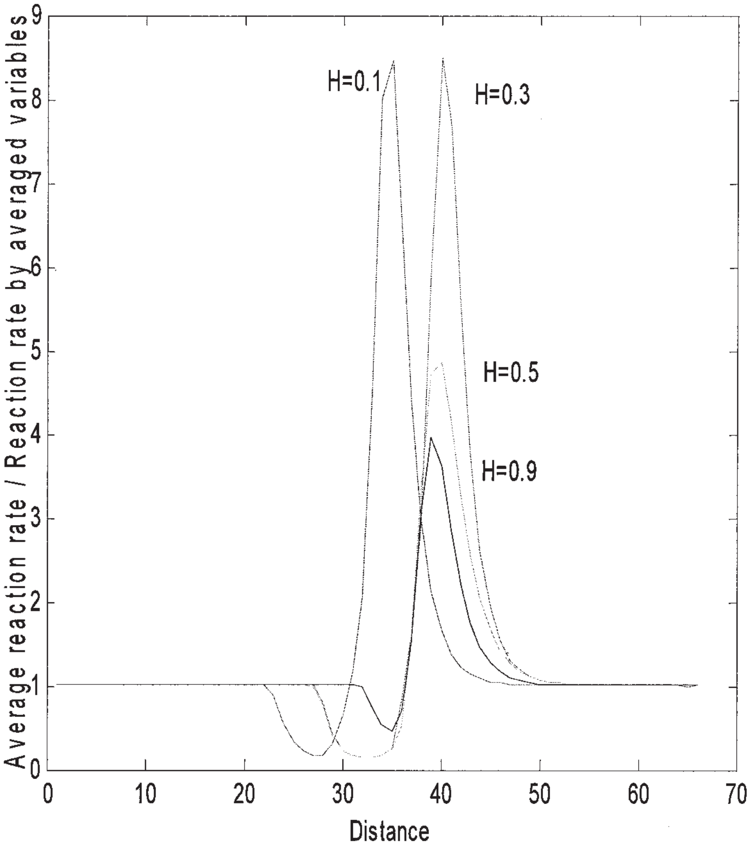

Figure 17. Spatial profiles of the ratio of the average reaction rate to the calculated reaction rate by averaged concentration, fuel density, and temperature for different values of the Hurst exponent of the fBm-distributed bond radius and for the parameters of Table 1 (thermal conductivity = 0.8635 W m^{-1} K^{-1}; velocity 432 m/day).

On the other hand, when for the same velocity the thermal conductivity is reduced by a factor of 10, the simulations give rise to much more distorted fronts. A typical example is shown in Figure 18, which plots the pore-radius field, the pressure, the temperature, the concentration, the conversion depth, and the reaction rate profiles for $H = 0.5$, for an injection velocity of 100 m/day. The effect of heterogeneity is somewhat different, here, compared to the random case. When spatial correlation is strong enough to give rise to connected (high or low) flow conductance regions, the induced flux differences can ultimately cause a curved front, assuming that the system is not under stoichiometric control, depending on the correlation length and the relative strength of dispersion. The higher the Hurst exponent, the closer the system behaves as layered, whereas at smaller values of H the deformation of the front is more limited. Likewise, there is less fluctuation in the oxidant profiles or the reaction rates. As the velocity decreases, the effect is weakened. The difference from the 1-D homogeneous behavior is akin to a process in a layered system, discussed below.

Layered Systems. A final example of heterogeneity to be discussed herein is a two-layered system, in which the pore-throat (bond) radius is different in the two layers. As shown in the previous section, the front velocity depends strongly on the oxidant flux. In a layered system, and in the absence of compressibility effects, or when the net gas generation is zero, the pressure gradients are the same in both layers. Thus, the mass flux in each layer would be proportional to the layer flow conductance (permeability). The reaction front in the high permeability region would initially propagate faster than that in the low permeability region, and soon will invade a cold unburned area. Then, the low permeability region will act as a heat sink for the faster front, the temperature of which will decrease. Assuming a system not under stoichiometric control (that is, for sufficiently high injection velocity), this brings a decrease in the consumption of oxidant, and in the front velocity. At the same time, because of transverse heat transfer (assuming that the layers are thermally coupled), the low permeability layer becomes preheated, resulting into a higher front temperature, a faster reaction rate, again for a kinetically controlled system, and a faster front velocity for the low-permeability layer, compared to the isolated case. Under certain conditions, the two velocities become equal and the fronts propagate at the same velocity. Akkutlu and Yortsos[35] considered the continuum analog of this problem, in which the fronts in the two layers were coupled only thermally. The authors found that the front in the lowest permeability layer controlled the coupled-front propagation (and could lead to extinction in the presence of heat losses, if the permeability ratio was sufficiently strong). In this section, we will use the numerical method we developed to study forward FC in a 2-D, two-layered system. In the simulations we used the parameters of Table 1, except that the thermal conductivity was reduced 10 times. A simplification of this problem in terms of two thermally thin layers coupled to one another is discussed in Akkutlu et al.[9]

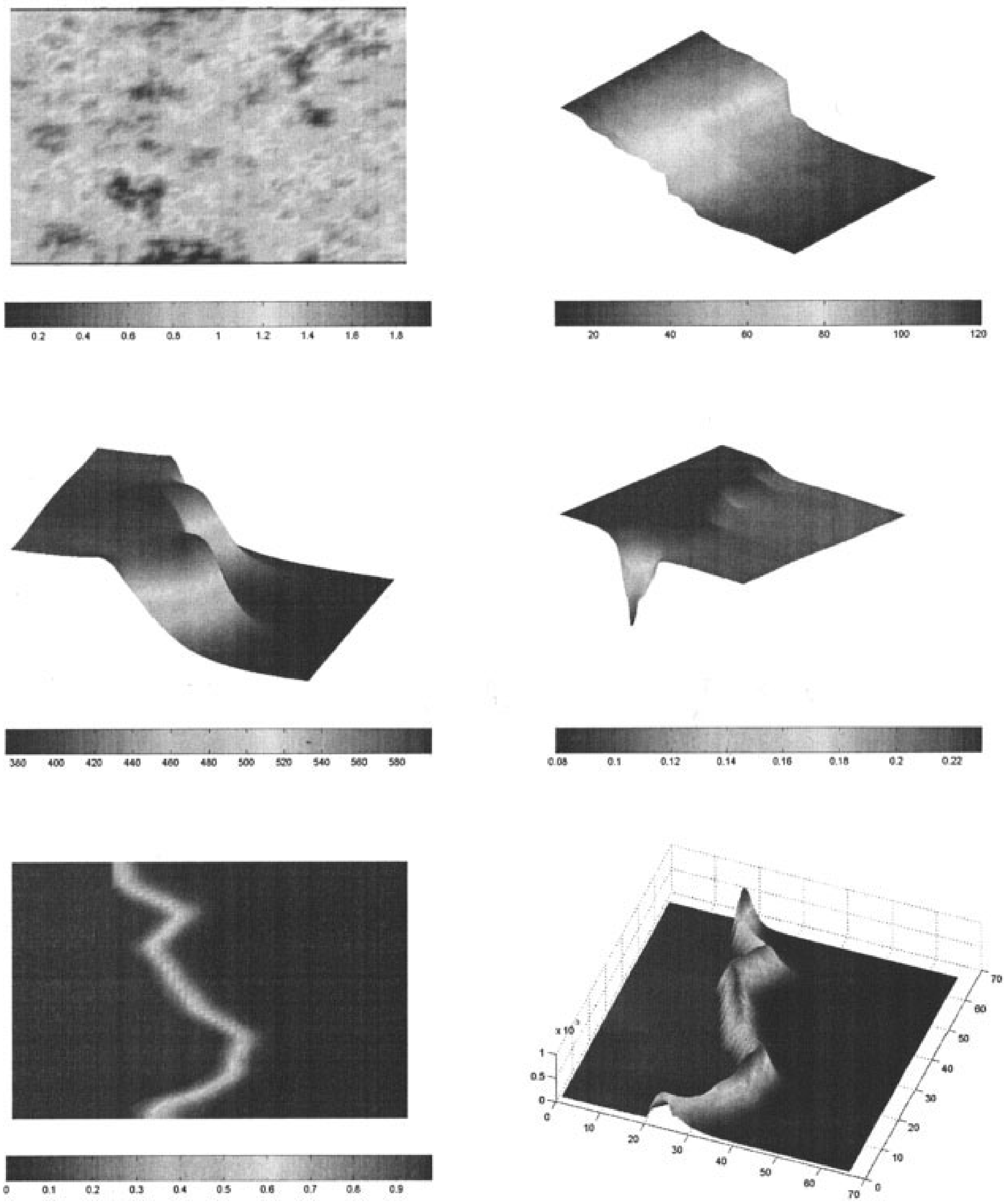

Figure 18. Spatial profiles of the bond radius, pressure, temperature, concentration, conversion depth efficiency, and the reaction rate profiles for fBm-distributed bond radii with *H* = 0.5 and injection velocity 100 m/day (thermal conductivity = 0.08635 W m^{-1} K^{-1}).

The adiabatic process in a layered system displays two different regimes: (1) coupled fronts with a common velocity, close to that of a homogeneous system corresponding to the low permeability; and (2) separated fronts moving at different speeds. Here, "separation of fronts" refers to the situation where the transverse mass and/or heat transfer is so weak that any coupling effect cannot be seen in the finite domain of our calculation. Once the fronts depart from each other, the distance between them increases with time (although ultimately, the transverse exchange of mass and energy will tend to couple the two fronts together).

Under conditions of kinetic control the fronts are coupled. Figure 19 shows the asymptotic state for a ratio of the pore throats in the two layers equal to 1.2, corresponding to a permeability ratio of about 2 (equal to 1.2^4). Mass and thermal dispersion are strong enough to retard the faster front and to accelerate the slower one. The elevated temperature and mole fraction in the high-permeability layer diffuse in the low-permeability region causing the coupling of the fronts. Because the oxygen is not completely consumed in either layer (in Figure 19 the lowest mole fraction is >0.1), the front velocity is determined by its temperature. The thermal energy conducted from the higher to the lower permeability layer is akin to a heat loss effect on the former, which results in front retardation, and to a preheating effect on the latter, resulting in front acceleration.

On the other hand, when the system is under conditions of stoichiometric control, the fronts separate. Figure 20 shows the results of simulations conducted under such conditions and for

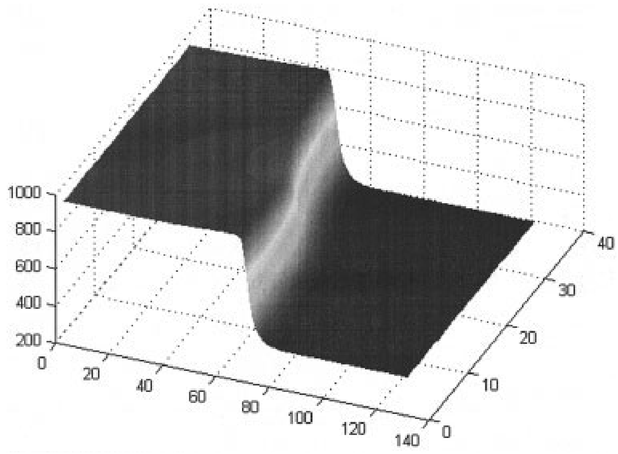

Figure 19. Profile of temperature (in degrees Kelvin) in the asymptotic state of adiabatic forward FC in a two-layered system using the parameters of Table 1 (thermal conductivity = 0.8635 W m^{-1} K^{-1}; velocity 832 m/day).

The permeability ratio is 2.0726 (1.2^4). The fronts in the two layers are coupled.

the same permeability ratio. Here, the parameters were varied such that the oxidant flux in each layer is sufficiently small, and all the oxidant reaching the front is completely consumed. Because in such cases the front velocity becomes independent of the front temperature (see Eq. 19) each front travels roughly in proportion to the velocity in each layer, thus leading to front separation. We must caution, however, that the separation observed in our simulations may be explained by the relatively small computational size of the domain. In reality, mass transfer will ultimately equalize the mole fractions across the layers and a coupling, albeit weak, will ultimately develop. The coupling of fronts in a layered system is further discussed in detail in Akkutlu and Yortsos[35] and in Akkutlu et al.[9]

Conclusions

In this article, we developed a pore-network model to study the dynamics of forward FC processes in porous media at the pore-network scale. Using a porous medium representation in terms of a dual network of sites and bonds, we developed a discrete pore-network model that encompasses a detailed description of the process at that scale. Because forward FC usually leads to traveling fronts, we implemented a novel moving coordinate method, which allows for the asymptotic state to be obtained in a straightforward manner. In the moving coordinates, the latter consists of steady-state profiles, in the case of homogeneous systems, and of fluctuating profiles in space, when properties, such as the pore-size distribution, are randomly distributed. The moving coordinate technique was validated using existing results in autocatalytic systems, whereas the overall formulation was validated using existing analytical results for 1-D systems. Because the pore-network formalism can also be viewed as a finite-difference analog of a continuum model (given the direct analogy between Poisseuille flow and Darcy's law), its results can be directly extrapolated to the continuum case as well.

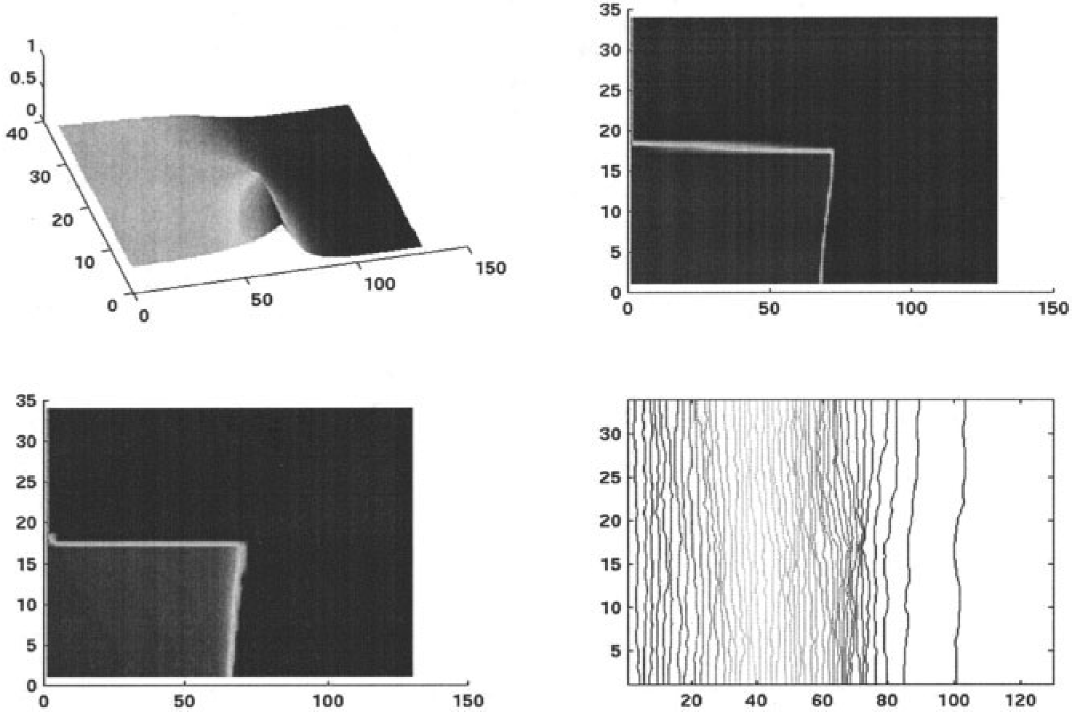

Figure 20. Profiles of dimensionless temperature, conversion depth, mole fraction, and pressure at the asymptotic state in adiabatic forward FC for a two-layered system using the parameters of Table 1 (but with thermal conductivity = 0.04 W m^{-1} K^{-1}; velocity 432 m/day; fuel density = 140 kg/m^3).

The permeability ratio is 2.0726 (1.2^4). The fronts in the two layers are separated.

The numerical method was used to successfully test recent analytical work for forward FC. The model reproduced multiple steady states in nonadiabatic cases with volumetric heat losses, as derived in the continuum model of Akkutlu and Yortsos.[8] In addition, we found an interesting effect, attributed to gas compressibility, when the heat losses are not of the volumetric type, but are applied on the lateral side of the domain. Because high-temperature regions receive a smaller mass flux because of reduced density, the asymmetry arising from the lateral heat losses is weakened, leading to flatter temperature profiles and a more uniform fuel consumption.

We used the numerical method to study the effect of the heterogeneity in the microstructure, introduced by the randomness in the pore radius. The local disorder generally leads to an uneven distribution of the oxidant flux, which results in less oxidant consumption, as compared to the homogeneous case. The underprediction in the oxidant consumption increases with an increase in the disorder (the width of the distribution), a decrease in the thermal conductivity, and a decrease in the spatial correlation. Temperature profiles are less sensitive, assuming sufficiently strong conduction. Shorter heat conduction lengths give rise to more oxygen leakage and rougher fronts. Temporary local extinction can emerge for sufficiently large injection rates. It was found that the spatially averaged reaction rate is generally very different than the rate calculated using the microscale Arrhenius expression, using the averaged variables, and discrepancies of a factor of 2 or higher were noted. Although the importance of this effect depends on the parameter values, it can be a cause of concern when the fronts at the small scale are sufficiently distorted. In all cases studied, the width of the front did not exceed 10 to 20 pores. In a correlated system, the front reached an asymptotic state, with a curved profile, which propagated in a coherent fashion. Using the simpler geometry of a two-layered system, we showed that combustion fronts can be coupled, assuming that there is sufficient oxidant supply to keep the system away from stoichiometric control. All these results imply that the microscale geometry can have a strong influence on the overall macroscopic behavior. For this reason, careful consideration should be given to the determination of the intrinsic combustion kinetics and their implementation in continuum models.

Acknowledgments

This research was partly supported by DoE contract DE-AC26-99BC11521, the contribution of which is gratefully acknowledged.

Literature Cited

1. Prats M. *Thermal Recovery*, SPE Monograph Series. New York, NY: Society of Petroleum Engineers of the American Institute of Mining, Metallurgical, and Petroleum Engineers; 1982.
2. Hwang S, Mukasyan AS, Rogachev AV, Varma A. Combustion wave microstructure in gas solid reaction systems: Experiments and theory. *Combust Sci Technol*. 1997;123:165-184.
3. Hwang S, Mukasyan AS, Varma A. Mechanisms of combustion wave propagation in heterogeneous reaction systems. *Combust Flame*. 1998; 115:354-363.
4. Aldushin AP. New results in the theory of filtration combustion. *Combust Flame*. 1993;94:308-320.
5. Schult DA, Matkowsky BJ, Volpert VA, Fernandez-Pello AC. Forced forward smolder combustion. *Combust Flame.* 1996;104:1-26.
6. Aldushin AP, Matkowsky BJ. Instabilities, fingering and Saffman–Taylor problem in filtration combustion. *Combust Sci Technol*. 1998; 13:293-341.
7. Aldushin AP, Rumanov IE, Matkowsky BJ. Maximal energy accumulation in a superadiabatic filtration combustion wave. *Combust Flame*. 1999;118:76-90.
8. Akkutlu IY, Yortsos YC. The dynamics of in-situ combustion fronts in porous media. *Combust Flame*. 2003;133:229-247.
9. Akkutlu IY, Yortsos YC. *Soc. Pet. Eng. J.*, submitted 2005.
10. Zik O, Moses E. Fingering instability in combustion: An extended view. *Phys Rev E*. 1999;60:518-531.
11. Conti M, Marconi UMB. Fingering in slow combustion. *Physica A*. 2002;312:381-391.
12. Xu B, Yortsos YC, Salin D. Invasion percolation with viscous forces. *Phys Rev E*. 1998;57:739-751.
13. Edwards DA, Shapiro M, Brenner H. Dispersion and reaction in two-dimensional model porous media. *Phys Fluids A*. 1993;5:837-848.
14. Edwards BF. Poiseuille advection of chemical reaction fronts. *Phys Rev Lett*. 2002;89:104501.
15. Miralles-Wilhelm F, Gelhar LW, Kapoor V. Stochastic analysis of oxygen-limited biodegradation in three-dimensionally heterogeneous aquifers. *Water Resour Res*. 1997;33:1251-1263.
16. Blunt MJ, Jackson MD, Piri M, Valvatne PH. Detailed physics, predictive capabilities and macroscopic consequences for pore-network models of multiphase flow. *Adv Water Resour*. 2002;25:1069-1089.
17. Satik C, Yortsos YC. A pore-network study of bubble growth in porous media driven by heat transfer. *J Heat Transfer*. 1996;118:455-462.
18. Prat M. Recent advances in pore-scale models for the drying of porous media. *Chem Eng J*. 2002;86:153-164.
19. Hoefner ML, Fogler HS. Role of acid diffusion in matrix acidizing of carbonates. SPE Paper 13564; 1985.
20. Sahimi M, Tsotsis TT. A percolation model of catalyst deactivation by site coverage and pore blockage. *J Catal*. 1985;96:552-562.
21. Mann R. Catalyst deactivation by coke deposition: Approaches based on interactions of coke laydown with pore structure. *Catal Today*. 1997;37:331-349.
22. El-Nafaty UA, Mann R. Support-pore architecture optimization in FCC catalyst particles using designed pore networks. *Chem Eng Sci.* 1999;54:3475-3484.
23. Lu C, Yortsos YC. *Ind Eng Chem Res*. 2004;43:3008-3018.
24. Lu C. *Modeling of Filtration Combustion at the Pore-Network Level*. PhD Dissertation. Los Angeles, CA: University of Southern California; 2003.
25. Akkutlu IY. *Dynamics of Combustion Fronts in Porous Media*. PhD Dissertation. Los Angeles, CA: University of Southern California; 2002.
26. Lu C, Yortsos YC. *Phys. Rev. E.* submitted 2005.
27. Libby PA, Blake TR. Theoretical study of burning carbon particles. *Combust Flame*. 1979;36:139-169.
28. Howell JR, Hall MJ, Elley JL. Combustion of hydrocarbon fuels within porous inert media. *Prog Energy Combust Sci*. 1996;22:121-145.
29. Niessen WR. *Combustion and Incineration Processes*. New York, NY: Marcel Dekker; 2002.
30. Ohlemiller TJ. Modeling of smoldering combustion propagation. *Prog Energy Combust Sci.* 1985;11:277-310.
31. Issa RI, Gosman AD, Watkins AP. The computation of compressible and incompressible recalculating flows by a non-iterative implicit scheme. *J Comput Phys.* 1986;62:66-82.
32. Issa RI, Ahmadi-Befrui B, Beshay KR, Gosman AD. Solution of the implicitly discretised reacting flow equations by operator splitting. *J Comput Phys*. 1991;93:388-410.
33. Chen CY, Meiburg E. Miscible displacements in capillary tubes. Part 2. Numerical simulations. *J Fluid Mech*. 1996;326:57-90.
34. Peitgen HO, Saupe D, eds. *The Science of Fractal Images*. New York, NY: Springer-Verlag; 1986.
35. Akkutlu IY, Yortsos YC. The effect of heterogeneity on in-situ combustion: The propagation of combustion fronts in layered porous media. SPE Paper 75128; 2002.

Manuscript received Oct. 20, 2003, and revision received July 26, 2004.